



Organic modification of montmorillonite with low molecular weight polyethylene glycols and its use in polyurethane nanocomposite foams

Nihal Sarier^{a,*}, Emel Onder^{b,1}

^a Faculty of Engineering and Architecture, Istanbul Kultur University, Atakoy Campus, Bakirkoy 34156, Istanbul, Turkey

^b Faculty of Textile Technologies and Design, Istanbul Technical University, Inonu Street, Gumussuyu 34437, Istanbul, Turkey

ARTICLE INFO

Article history:

Received 17 March 2010

Received in revised form 30 May 2010

Accepted 4 July 2010

Available online 2 August 2010

Keywords:

Nanocomposite

Organoclay

Polyurethane

PEG

XRD

DMA

ABSTRACT

This paper deals with the preparation of organoclays by intercalating poly(ethylene glycol) molecules (PEG) between Na montmorillonite (Na-MMT) layers in a clay-water suspension system. X-ray diffraction (XRD) results of organoclays revealed that galleries of MMT were expanded after their intercalation with three different low molecular weight PEGs, including PEG600, PEG1000 and PEG1500. Thus, the distance of the interlayer spacing of MMT, $d = 1.38$ nm, was increased to $d = 1.72$, 1.75 and 1.69 nm, respectively, in the organoclay samples. The results of Fourier transform infrared spectroscopic (FTIR), thermogravimetric (TG) and scanning electron microscopic (SEM) analyses supported the findings of XRD and implied that the clay mineral mainly lost its hydrophilic character and gained organophilic features. The organoclay samples also presented improved thermal stabilities. In addition, polyurethane rigid nanocomposite foams composed of 2% organoclays were synthesized, and the effects of the organoclays on the thermal and mechanical performance of the nanocomposite foams were investigated.

© 2010 Elsevier B.V. All rights reserved.

1. Introduction

Polymer–clay nanocomposites are prepared by dispersing layered clay minerals into polymers. As a new class of polymers, they have drawn considerable attention due to their significantly enhanced properties compared to traditional polymers, such as heat and flame resistance [1–4], mechanical strength [5,6], gas barrier resistance [7–10], thermal stability [11–13], biodegradability [14,15] and ionic conductivity [16,17]. Some of these nanocomposites are now applied commercially in automotive (e.g., gas tanks, bumpers, interior and exterior panels), construction (e.g., building sections and structural panels), aerospace (e.g., flame retardant panels and high performance components), electrical (e.g., electrical components and printed circuit boards), and beverage and food packaging applications, as well as in protective coatings and adhesive molding compounds [18–25].

The ultimate aim of fabricating high performance polymer–clay nanocomposites is to separate and disperse individual anisotropic clay particles within the polymer matrix. In the manufacture of polymer–clay nanocomposites, an extensively used clay mineral is montmorillonite (MMT). However, MMT is not compatible with hydrophobic polymers due to the cohesive forces of the clay

particles; therefore, chemical modification techniques have been applied to give the clay organophilic character while expanding the clay layers as much as possible prior to the nanocomposite manufacture [26,27]. Commercially available organophilic clays are widely produced by the exchange of metal cations in MMT galleries with organic ammonium salts [28]. The organoclays prepared with organic ammonium salts are not very suitable for some engineering applications like melt processing, since they undergo thermal degradation above 170–180 °C [29]. For that reason, research interest has shifted toward the use of thermally stable organic modifiers such as phosphonium or imadazolium salts in organoclay production [30–32]. The latter chemicals do have some disadvantages, i.e., low solubility in water and high cost, and this limits their penetration into the organoclay market [33].

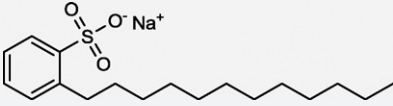
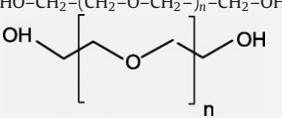
Polyethylene glycols (PEGs), also referred to as polyoxyethylenes, are composed of repeating dimethyl ether chains with hydroxyl ending groups, $\text{HO}-\text{CH}_2-(\text{CH}_2-\text{O}-\text{CH}_2)_n-\text{CH}_2-\text{OH}$, and accordingly possess dual features of water solubility and organic solubility. They are well-known nonionic surfactants that are chemically and thermally stable, biodegradable, non-toxic, non-corrosive and inexpensive [34,35]. The adsorption behavior of PEG with MMT in aqueous and melt systems has been reported to operate through different mechanisms. One mechanism suggests the major driving forces for PEG adsorption on smectite as hydrophobic interactions between $-\text{CH}_2$ chains and silica layers and hydrogen bonding between the ether oxygen atoms of PEG and $-\text{OH}$ groups [36,37]. The other mechanism suggests that

* Corresponding author. Tel.: +90 2124984488; fax: +90 2124658308.

E-mail addresses: n.sarier@iku.edu.tr (N. Sarier), onderem@itu.edu.tr (E. Onder).

¹ Tel.: +90 2122518808; fax: +90 2122588829.

Table 1
Chemical compounds used in preparation of the organoclay (OC) samples.

Chemical agent	IUPAC name	Molecular formula	Structural formula	Molar mass (g mol ⁻¹)	Function in reaction
SDS	Sodium salt of 4-dodecylbenzene sulfonic acid	CH ₃ (CH ₂) ₁₁ C ₆ H ₄ SO ₃ ⁻ Na ⁺		348.49	Anionic surfactant for dispersing the clay in colloidal system
PEG600 (n = 4) PEG1000 (n = 5–7) PEG1500 (n = 8–9)	Poly (oxy ethylene)	HO-CH ₂ -(CH ₂ -O-CH ₂) _n -CH ₂ -OH		570–630 950–1050 14,001,600	Intercalants in organoclay production
		Average chain length n = 4 1.738 nm n = 6 2.310 nm n = 9 3.168 nm			

the adsorption is an entropy-driven process [38]. A number of researchers have studied the melt intercalation of high molecular weight PEGs, 20,000–400,000 g mol⁻¹, in MMT and have succeeded to some extent at intercalating and exfoliating MMT nanocomposite structures [26,34–46]. The comparison of melt intercalation with solution intercalation was studied, and the clay galleries expanded from 0.47 to 0.83 nm following both melt intercalation and solution intercalation [39]. Research on the use of PEGs in both melt and solution intercalation processes for MMT has been extensive [47,48] and still requires attention to develop effectively intercalated and thermally stable new organoclay products using PEGs, which may be of interest in the current market.

In the present study, we aimed to develop organoclays by intercalating PEG molecules into Na-MMT minerals in a colloidal dispersion, as well as to synthesize polyurethane rigid nanocomposite foams incorporated with the modified organoclay by in situ polymerization of 1,3-propanediol and toluene-2,4-diisocyanate. Herein, relatively small molecular weight PEGs – PEG600, PEG1000 and PEG1500 – were used in the organoclay production. In addition to structural and thermal characterization of the organoclays, their actual contribution to the thermal and mechanical performance of the polyurethane rigid nanocomposite foams was also examined. The organoclays and polyurethane nanocomposites were characterized by X-ray diffraction, Fourier transform infrared spectroscopy, thermogravimetry and scanning electron microscopy integrated with an energy dispersing spectrometer.

2. Experimental

2.1. Materials

Na-MMT, named Nanocor[®] (NC), was purchased from AMCOL Int. Company. Specific gravity of 2.6, aspect ratio of 200–400, pH (5% dispersion) of 9.5–10.5 and cation exchange capacity (CEC)

of 145 cmol kg⁻¹ were the listed physical properties of NC [50]. The particle size distribution of NC was measured with a Malvern Mastersizer 2000 at a 2.40 μm wavelength. The mean diameter was found to be 1.41 μm, and 90% of the particles were less than 2.81 μm. The materials and chemical reagents used in both the organoclay (OC) preparation and polyurethane (PU) production processes are summarized in Tables 1 and 2. The technical grade chemicals used in the experiments were obtained from Merck Co.

2.2. Preparation and characterization of the organoclay samples

Initially, 18 g of Na-MMT (NC) was mixed with 100 mL of 0.14 M SDS (aq.) at 1000 rpm for 60 min while keeping the temperature at 80 °C. Next, 30 wt% PEG was added to the colloidal dispersion and stirring was performed at 1500 rpm for the next 120 min. The PEG concentrations achieved were 500 mM of PEG600, 300 mM of PEG1000 and 200 mM of PEG1500. At the end of the organophilic modification, swollen colloidal samples were obtained.

The system was cooled to ambient temperature and then processed in a laboratory-type ultrasonic processor (Hielscher UP400S) for 30 min with an acoustic power density of the applied ultrasonic energy of 460 W cm⁻², amplitude of 210 μm and period of 0.8 s. The solid phase was then separated by centrifugation, washed and vacuum filtered. Finally, the obtained filter cake was vacuum dried at 65 °C for 8 h. The OC samples, namely OC600, OC1000 and OC1500, were ground with ultrasonication for 15 min under the conditions given above. The powdered samples were stored in closed plastic containers under ambient conditions.

The changes in the structure of MMT after organic modification were examined with a SHIMADZU XRD-6000 X-ray diffractometer (XRD) using Cu Kα radiation at a wavelength of 1.5405 Å. The applied voltage and current values were 40.0 kV and 30.0 mA, respectively. X-ray diffractograms were obtained at a scanning rate of 2.0000° min⁻¹, whereas the 2θ angles ranged between 2.0000°

Table 2
Chemical compounds used in the polyurethane foam production.

Chemical agent	IUPAC name	Molecular formula	Molar mass (g mol ⁻¹)	Function in reaction
TDI	4-Methyl-m-phenylene diisocyanate	2,4-(NCO) ₂ C ₆ H ₃ CH ₃	174.16	Monomer
Polyol	1,3-Propanediol	HO(CH ₂) ₃ OH	76.1	Monomer
DABCO	Triethylenediamine, 1,4-Diazabicyclo[2.2.2]octane	C ₆ H ₁₂ N ₂	112.18	Catalyst
Stannus octoate	Tin 2-Ethylhexanoate	[CH ₃ (CH ₂) ₃ CH(C ₂ H ₅)COO] ₂ Sn	405.10	catalyst
Silicone oil	–	–	–	Surfactant/stabilizer
Methylene chloride	Dichloromethane	CH ₂ Cl ₂	84.93	Blowing agent
Water	–	–	–	Blowing agent
MDI	Diphenylmethane 4,4-diisocyanate	C ₁₅ H ₁₀ N ₂ O ₂	250.26	Hardener

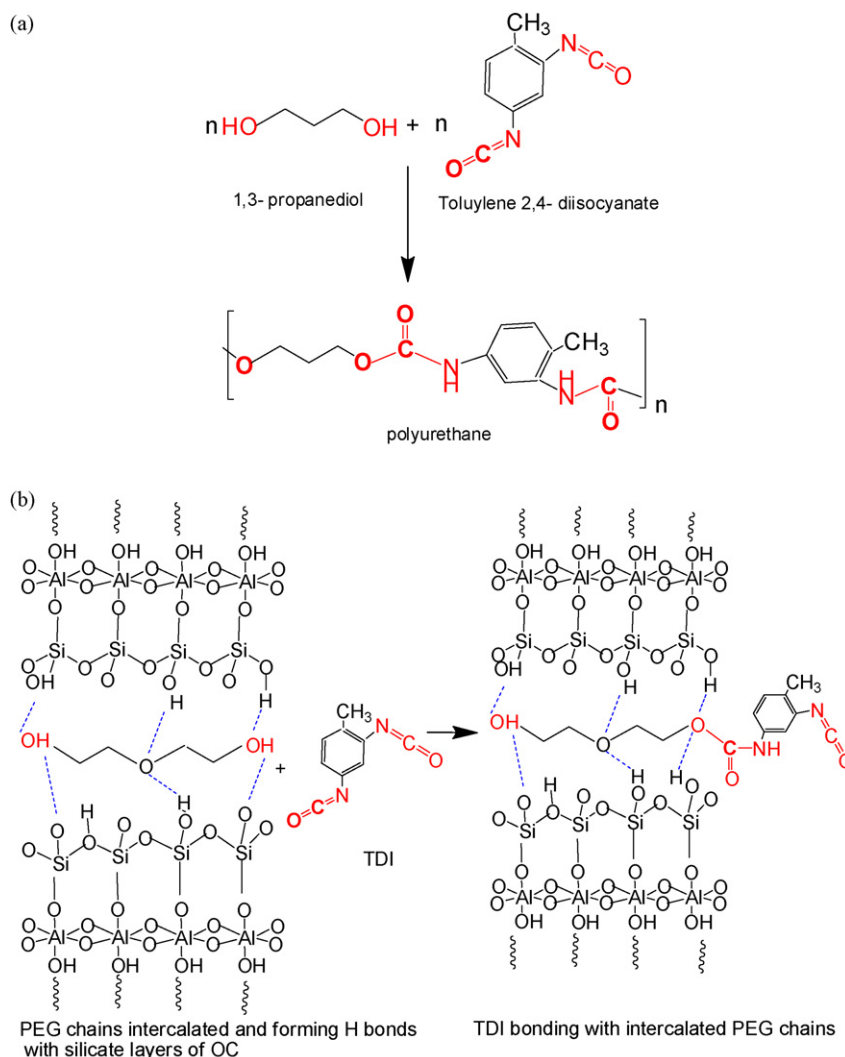


Fig. 1. (a) The major polymerization reaction between 1,3-propanediol and TDI and (b) the suggested interaction between TDI and PEG chains in OCs during PU nanocomposite foam synthesis.

and 70.0000° with a step scanning speed of $0.0200^\circ \text{ s}^{-1}$. The amount of each sample was constant at 250 mg. To identify the chemical structure of the organoclays, the infrared transmission spectra of the specimens dispersed in KBr pellets were acquired on a Perkin-Elmer Fourier transform infrared spectrometer (FTIR) in the range of $4000\text{--}450 \text{ cm}^{-1}$ at a resolution of 4 cm^{-1} . Thermogravimetric (TG) analyses were carried out with a Perkin-Elmer Pyris 1 TG. Approximately 15.0 mg samples in alumina crucibles were heated from 20 to 900°C under nitrogen flowing at 50 mL min^{-1} . The heating rate was $10^\circ\text{C min}^{-1}$. Scanning electron microscopy (SEM) and energy dispersive spectroscopy (EDS) of the samples were performed on a JEOL JXA 840A type EDS connected to an SEM instrument. For preparation of the SEM samples, approximately 0.01 g of a dried powdered clay sample was placed on standard mounts 15 mm in diameter and 2 mm in depth under a vacuum and then coated with a 1–2 nm thick conductive layer of gold to prevent charging prior to imaging.

2.3. Synthesis and characterization of PU–OC nanocomposite foams

The second part of the experimental work deals with the manufacture of four different polyurethane nanocomposite foams, each containing 2 wt% OC or NC. The produced nanocomposite rigid

foams were labeled as PU (control), PUNC (including 2 wt% NC), PUOC600 (including 2 wt% OC600), PUOC1000 (including 2 wt% OC1000) and PUOC1500 (including 2 wt% OC1500).

For production of the nanocomposites, 420.5 mmol of 1,3-propanediol and 2 wt% OC (or 2 wt% NC) were mixed and stirred at 1100 rpm and 20°C for 45 min in 75 mL plastic containers. While stirring, 91.9 mmol of TDI and 0.14 g of silicone oil were added to the polyol–clay mixture. Then, 0.012 g of DABCO and 0.036 g of stannus octoate were added as catalysts. The polymerization was carried out with constant stirring for 10 min. Finally, 0.2 g of MDI, 1 mL of methylene chloride and a few drops of water were added into the polymer mixture to finish the reaction. Foaming occurred with a violent exothermic reaction. The foam samples were allowed to cure for 1 week at room temperature. The major polymerization reaction of PU is given in Fig. 1a, and the interaction between PU–OC in the nanocomposite structure is suggested to be as shown in Fig. 1b.

PU nanocomposites were examined by TG and SEM-EDS under the conditions detailed above. To determine the effect of OC on the compression behavior of the PUOC nanocomposites, PU (control) and PUOC600 were tested on a METTLER TOLEDO dynamic mechanical analyzer (DMA/SDTA861) using the large compression module with an applied force (F) that ranged from 1 to 10 N at 1 Hz and 25°C .

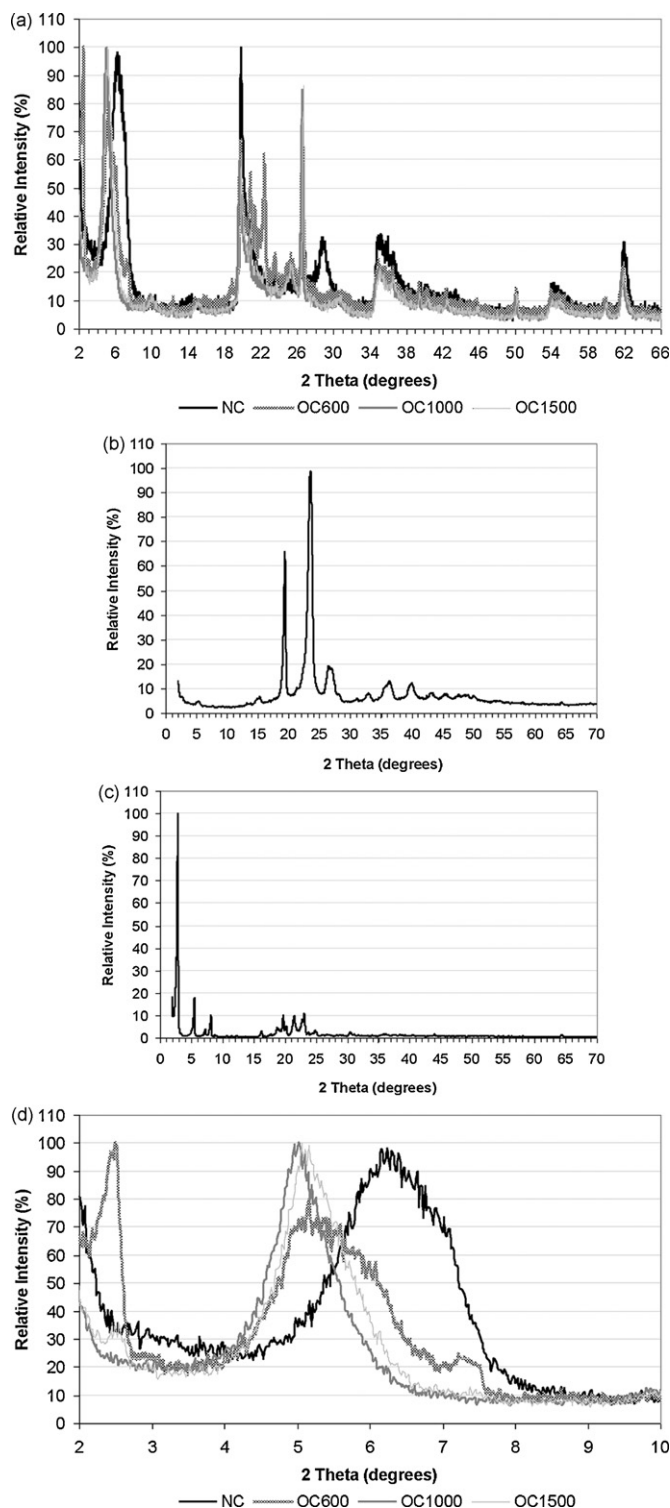


Fig. 2. X-ray diffraction patterns of (a) NC, OC600, OC1000, OC1500, (b) PEG1500, (c) SDS and (d) all samples for $2\theta = 2.00\text{--}10.00^\circ$.

3. Results and discussion

3.1. XRD results of OC samples

Fig. 2a and d shows the typical reflections obtained from the X-ray diffraction patterns of NC, OC600, OC1000, OC1500, PEG1500 and SDS. NC gave the four strongest reflections at 2θ angles of 6.38° , 19.92° , 26.66° and 35.02° , corresponding to the characteristic

reflections of the MMT mineral [26,27]. The reflection at $2\theta = 6.38^\circ$ indicated that the interlayer spacing between the $\{001\}$ planes of NC was $d = 1.38$ nm. This reflection shifted to $2\theta = 5.12^\circ$, 5.06° and 5.22° in the X-ray diffractograms of OC600, OC1000 and OC1500, respectively; therefore, the corresponding interlayer spacings were increased to $d = 1.72$, 1.75 and 1.69 nm, respectively, which was evidence of the successful intercalation of MMT with PEG molecules. Together with the shifting, a broadening took place in the diffractogram of OC600 between $2\theta = 4.54^\circ$ and 7.35° , and the reflection at $2\theta = 7.88^\circ$ ($d_{002} = 1.12$ nm) observed in the pattern of NC moved to $2\theta = 7.35^\circ$ ($d_{002} = 1.21$ nm) in that of OC600, implying strong interactions between the intercalating molecules and the clay galleries [49].

The XRD pattern of PEG1500, which showed three main reflections at 19.31° ($d = 0.46$ nm), 23.43° ($d = 0.38$ nm) and 26.71° ($d = 0.33$ nm), was different than that of OC1500. In fact, the typical reflections of PEG chains [35,36] in the PEG1500 X-ray diffractogram did not appear as individual reflections in the XRD of OC1500. This indicated that the adsorbed or free PEG1500 on the clay surface was negligible, and that the polymer chains in the montmorillonite galleries were mainly intercalated while the crystallization of the PEG molecules in OC1500 was hindered [43,44]. The XRD pattern of OC1000 mostly overlapped with that of OC1500, signifying similar structural changes.

Moreover, the changes in XRD patterns of all of the OC samples between $2\theta = 18.00^\circ$ and 40.00° indicated the intercalation of MMT. The significant intensity decreases and slight shifts in the typical MMT reflections at $2\theta = 19.92^\circ$, 26.66° , 28.72° and 35.34° , observed as broadening in the organoclay patterns, were also attributable to delamination and disorientation of clay platelets [35,40]. On the other hand, several reflections in the XRD pattern of OC600 at $2\theta = 2.45^\circ$ and between $2\theta = 20.00^\circ$ and 25.00° were most likely due to the existence of residual SDS in that particular sample.

3.2. FTIR results of OC samples

Fig. 3a and b illustrates the spectra obtained from FTIR analyses. The asymmetric stretching vibration (ν_3) of structural -OH groups in MMT at 3630 cm^{-1} shifted to 3622 cm^{-1} in the spectra of OC samples, indicating a decrease in O–H bond strength upon intercalation. Bending in plane vibrations of -OH groups (ν_2), characterized by a broader band, were slightly shifted from 1642 to $1640\text{--}1639\text{ cm}^{-1}$ as a result of a decrease in the number of -OH groups. Moreover, the broad band observed at 3436 cm^{-1} , corresponding to the overlapping symmetrical stretching vibrations (ν_1) of both structural and free -OH groups, was shifted to $3449\text{--}3446\text{ cm}^{-1}$, which was due to the bonding of $\text{-CH}_2\text{-(CH}_2\text{-O-CH}_2\text{)-CH}_2\text{-}$ chains with Si–O–Si and Al–O–Al sites [27,39,42].

Bands at 2921 and 2853 cm^{-1} , due to stretching vibrations of -CH_2 groups in the PEGs, also appeared in spectra of the OC samples. A -CH_2 bending band at 1467 cm^{-1} and -CH rocking band at 1351 cm^{-1} from the PEG chains were also noted as distinct peaks in the spectra of OC600, OC1000 and OC1500. The peaks at 1298 , 1108 and 952 cm^{-1} were related to C–O–C stretching vibrations of ether groups in the PEG chains, and overlapped with the stretching vibrations of Si–OH or Al–OH groups in MMT, which resulted in peak broadening. The IR peaks of NC observed in the range of $1039\text{--}467\text{ cm}^{-1}$ were assigned to the stretching and bending vibrations of Si–O–Al, Si–O–Si and Al–O groups in MMT. These bands became remarkably broadened in the spectra of OC600, OC1000 and OC1500. The Si–O–Si out of plane stretching peak of NC at 1039 cm^{-1} was shifted to 1044 cm^{-1} in the spectra of all OC samples, which was attributed to alteration of the environment of the Si–O–Si groups due to the presence of organic chains as a result of the intercalation of PEG molecules [36,37,46].

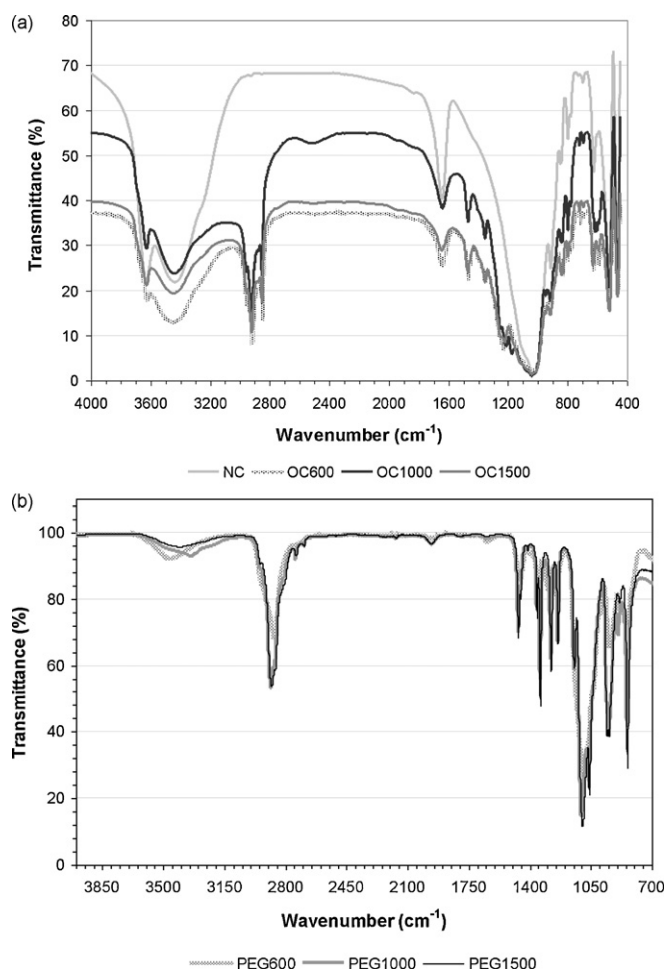


Fig. 3. FTIR transmission spectra of (a) NC, OC600, OC1000, OC1500 and (b) PEG600, PEG1000, PEG1500.

3.3. Thermal analyses of OC samples

TG curves and the corresponding derivative curves (DTG) of PEG molecules and NC, OC600, OC1000 and OC1500 are presented in Fig. 4a and b. In these graphs, the thermogravimetric behavior of organoclay samples and the materials used in their production are given. Thus, the mass loss percentages and their rates are plotted against temperature for comparison.

The thermal analysis of NC demonstrated the typical behavior of Na-MMT [51]. The dehydration of water molecules adsorbed in pores and clay galleries took place within the temperature range from room temperature to 300 °C, such that the first endothermic peak appeared at 85 °C in the DTG graph of NC, and the corresponding mass loss was 12% at about 110 °C. Above this temperature up to 300 °C, the mass loss decelerated greatly and stopped at 14%. Furthermore, there was no significant mass loss between 300 and 500 °C. The thermal degradation accelerated again after 500 °C and continued up to 850 °C, which was related to the dehydroxylation of –OH groups bonded to the octahedral Al³⁺ and tetrahedral Si⁴⁺ groups of the MMT [24]. The following step was associated with the destruction of the mineral structure. The residue at 850 °C was 82%.

PEG600, PEG1000 and PEG1500 displayed very similar thermogravimetric behaviors upon heating. In general, their thermal decomposition mostly occurred in the range of 275–435 °C, with a maximum at 420 °C. For PEG600, the mass loss was initially rapid, probably because of the presence of more hydroxyl groups in the structure, which was similar to the behavior observed by FTIR analysis (see Fig. 3b).

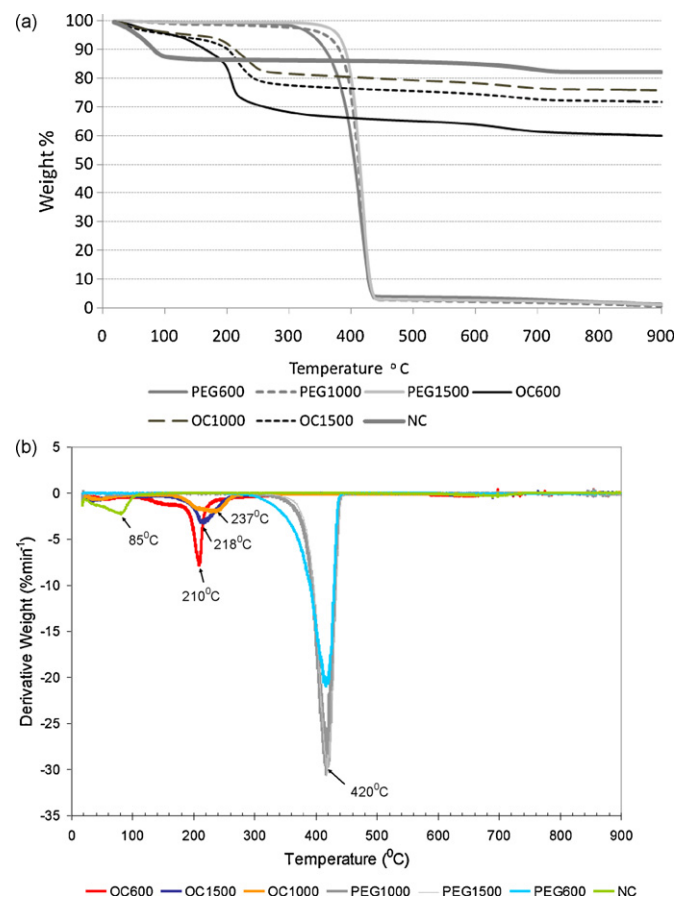


Fig. 4. Thermogravimetry results of PEGs and organoclay samples: (a) TG curves and (b) DTG curves.

The thermal degradation of OC samples differed significantly from that of NC in the temperature range from 25 to 300 °C. The dehydration peaks disappeared in the DTG graphs of OC samples, and the mass loss in each TG graph was reduced to 4% at 110 °C. These findings implied a conversion from hydrophilic to organophilic character in the structures of OC600, OC1000 and OC1500. PEG molecules, intercalated in the galleries, appeared to degrade mainly in the range of 180–270 °C, where the maximum mass loss rates occurred at 210, 218 and 237 °C, respectively. At the end of this step, the mass loss percentages of OC600, OC1000 and OC1500 were 30, 18 and 22%, respectively. In the following steps from 300 to 500 °C, as well as from 500 to 850 °C, the TG curves of OC samples tended to follow paths more or less parallel to that of NC, indicating the inorganic character of the residues. Moreover, no peak was observed in the DTG curves of OC samples related to possible free surface PEG molecules. This attainable thermal stability of OC samples suits the conditions required in many polymer composite manufacture routes [23]. Residues at 850 °C, roughly 60% for OC600, 76% for OC1000 and 72% for OC1500, were also distinctive, explaining the permanent structural modifications of the clays, although they retained their inorganic character.

3.4. Surface characteristics of OC samples

The surface morphologies of NC and OC specimens were examined based on SEM photographs. The sphere of distinct grains of NC shown in Fig. 5a disappeared in OC samples, as shown in Fig. 5b–d. Lateral displacements of silicate layers were quite prominent, and individual flakes with different aspect ratios were partially separated or distributed randomly.

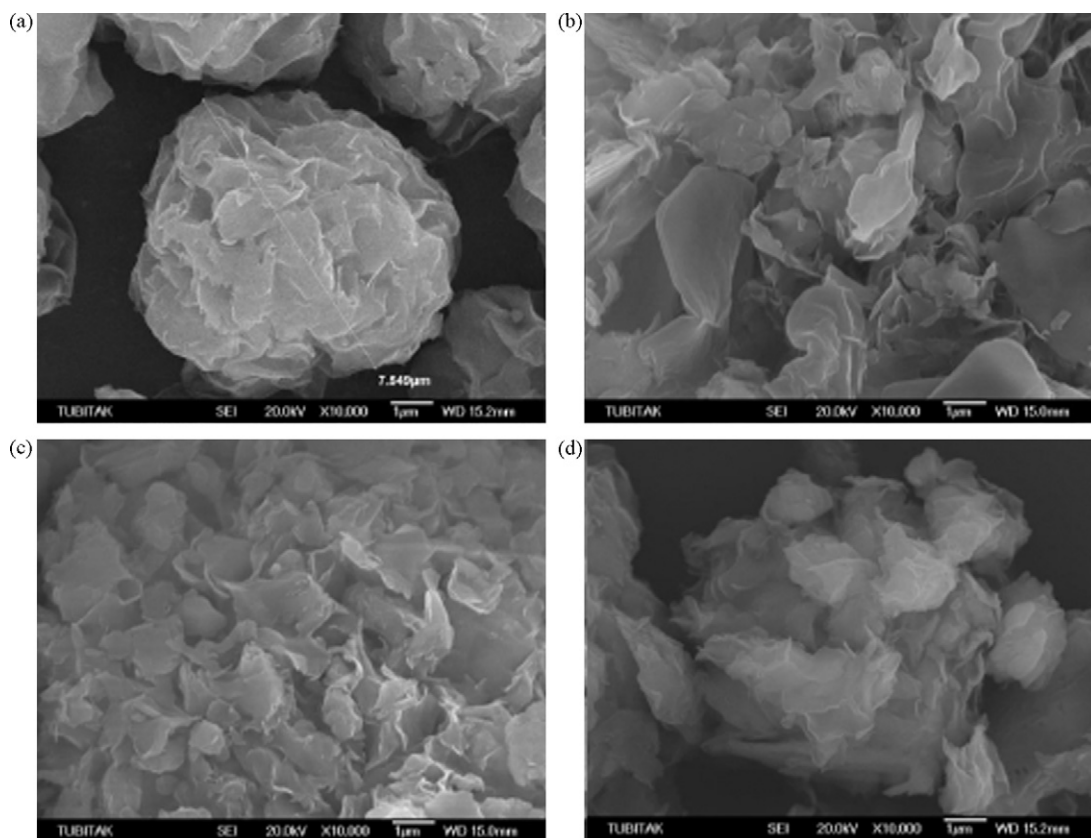


Fig. 5. SEM photographs of NC and OC samples (magnifications 10,000 \times ; 20 kV): (a) NC, (b) OC600, (c) OC1000 and (d) OC1500.

3.5. Measured properties of PUOC nanocomposite foams

The TG-DTG analyses of all PU foams exhibited four decomposition steps. The improvements in the thermal degradation behavior of PU nanocomposite foams modified by incorporating 2% NC, or alternately 2% OC600, 2% OC1000 and 2% OC1500, are shown in Table 3.

PU (control) foam showed a thermal stability up to 207 °C, where the mass loss was quite small (4%) and was related with dehydration and the evaporation of free surfactants entrapped in the foam structure. Afterward, the mass loss due to thermal degradation of the organic chains accelerated and attained a maximum at 317 °C, such that the total mass loss was 47% at 349 °C.

In PUNC containing 2%NC, the first step of thermal decomposition occurred in the range of 241–326 °C, with a maximum mass loss rate at 295 °C, diverging from that of pristine PU. However, the temperatures corresponding to 5 and 10% mass losses were quite similar for both PU and PUNC. The main advantage of this structure was a postponed mass loss in the second stage of thermal decomposition. Additionally, it gave the highest residue (32%)

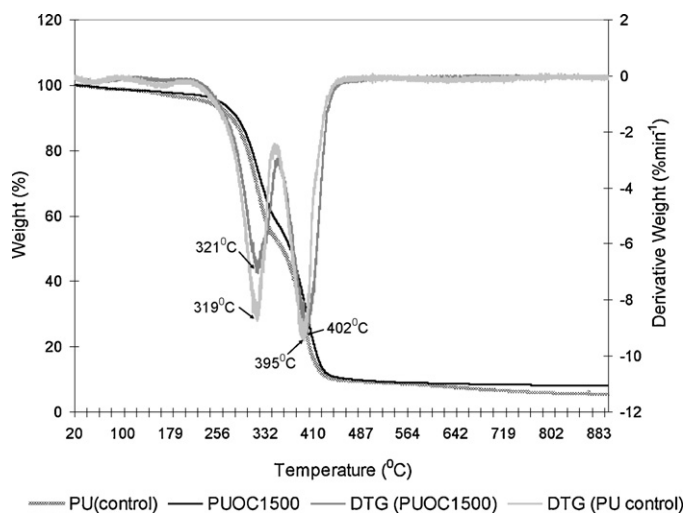


Fig. 6. TG-DTG curves of PU (control) and PUOC1500.

Table 3

The comparison of TG results of PU (control), PUNC and PUOC nanocomposite foams.

Sample	T (°C) at 5% mass loss	T (°C) at 10% mass loss	1st step			2nd step			Residue% at 400 °C	Residue% at 900 °C
			$T_{\text{start}} - T_{\text{end}}$ (°C)	Mass loss%	T_{peak} (°C)	$T_{\text{start}} - T_{\text{end}}$ (°C)	Mass loss%	T_{peak} (°C)		
PU (control)	237	278	207–349	43	319	349–380	44	395	23	5
PUNC	237	275	241–326	27	295	326–420	60	396	32	10
PUOC600	262	288	250–351	41	329	351–446	40	396	25	6
PUOC1000	244	282	252–351	46	348	351–446	42	399	26	8
PUOC1500	257	286	255–351	39	321	351–450	49	402	30	7

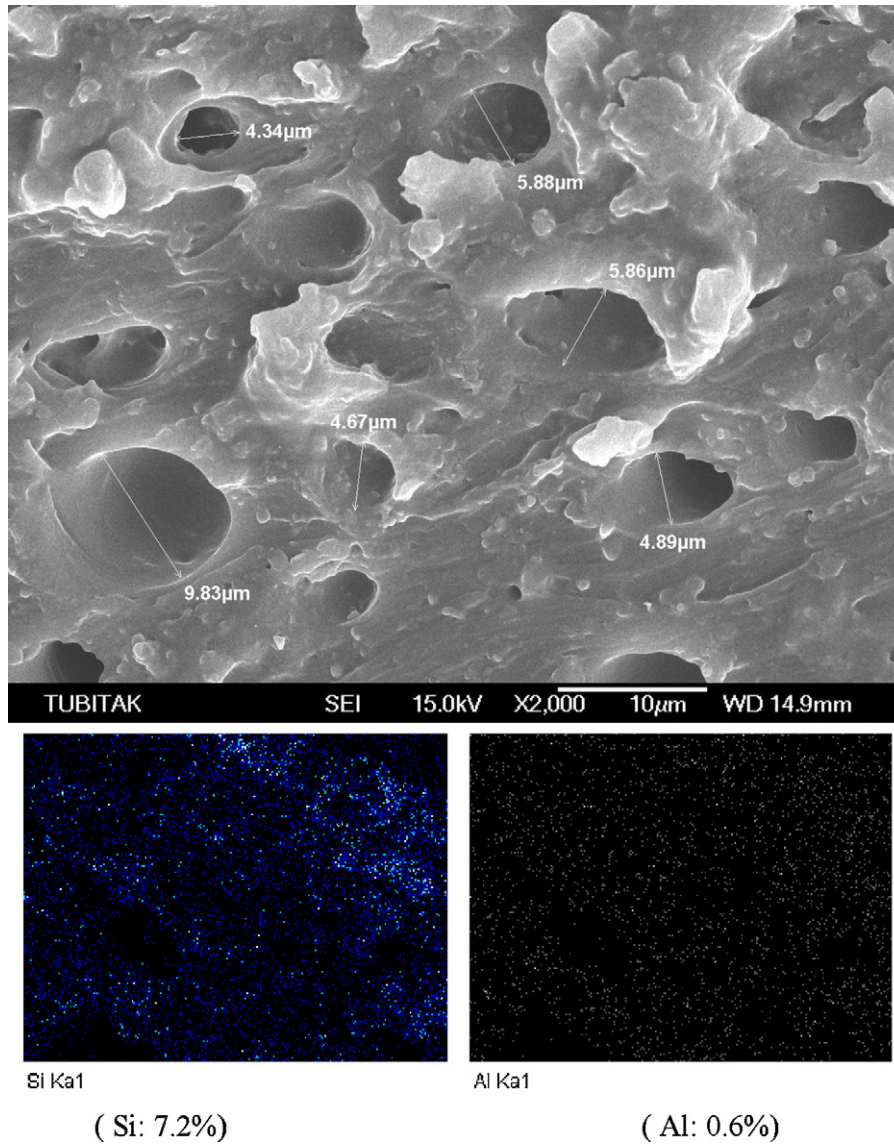


Fig. 7. SEM photograph and related EDS mappings of PUOC1000.

of all of the samples at 400 °C, probably because NC acted mainly as an inorganic filler in the body [52,53]. Conversely, the thermal stability of PUOC nanocomposite foams, PUOC600, PUOC1000 and PUOC1500, was improved in both the low and high temperature regions, as given in Table 3. The temperatures corresponding to 5% and 10% mass losses were shifted toward higher values by 7–15 and 4–10 °C, respectively. The onset temperatures of thermal decompo-

sition in the first stages of the TG curves of PUOC600, PUOC1000 and PUOC1500 were shifted to 250–255 °C, considerably higher than that of PU (control). At the end of this stage at 351 °C, the mass percentages of PUOC600, PUOC1000 and PUOC1500 were 59, 54 and 61%, respectively, all greater than the residual mass percentage of PU. The second stage thermal decomposition ended at 446–450 °C, 66–70 °C higher than that of PU (control).

Table 4
DMA results of PU (control) and PUOC600 foams.

F [N]	PU (control) ($\rho = 325 \text{ kg m}^{-3}$)		PUOC600 (1st synthesis) ($\rho = 325 \text{ kg m}^{-3}$)		PUOC600 (2nd synthesis) ($\rho = 300 \text{ kg m}^{-3}$)	
	E' [MPa]	$\tan \delta$	E' [MPa]	$\tan \delta$	E' [MPa]	$\tan \delta$
1.00	3.67	0.13	5.29	0.09	8.53	0.10
2.00	3.98	0.15	5.31	0.11	9.03	0.11
3.00	4.62	0.15	5.37	0.12	9.40	0.12
4.00	5.28	0.14	5.82	0.15	9.86	0.11
5.00	5.89	0.14	6.52	0.14	11.04	0.12
6.00	6.31	0.14	6.88	0.13	11.93	0.11
7.00	6.94	0.14	6.90	0.12	11.98	0.11
8.00	6.87	0.14	6.80	0.12	11.92	0.11
9.00	6.76	0.14	6.63	0.12	11.77	0.11
10.0	6.74	0.13	6.57	0.12	11.74	0.11

Fig. 6 highlights the differences in the TG-DTG curves of PU (control) and PUOC1500.

The residues of the nanocomposites were 25–30% at 400 °C and 6–8% at 900 °C, all greater than that of the PU control, indicating the successful dispersion and binding of organoclays in the PU matrices. EDS mapping of PUOC1000 supported efficient dispersion of the organically modified clay in the host PU foam by in situ polymerization, where the guest Al and Si atoms were randomly and evenly distributed throughout the body at comparable levels (see Fig. 7).

Table 4 summarizes the values of elastic modulus (E') and loss factor ($\tan \delta$), defined as the ratio between the loss modulus (E'') and elastic modulus (E'), for samples PU and PUOC600, which had similar densities (300–325 kg m⁻³). The results clearly showed that 2% organoclay content in the composite structure caused considerable increases in elastic modulus (E') values of the samples at almost every compression level from 1 to 10 N, as well as decreases in the values of $\tan \delta$, indicating a shift from viscoelastic to elastic behavior.

4. Conclusion

In the present study, we showed that small molecular weight PEGs, including PEG600, PEG1000 and PEG1500, could be successfully intercalated into Na-MMT in a colloidal dispersion system. XRD analyses revealed that the interlayer spacing of NC expanded from 1.38 to 1.72, 1.75 and 1.69 nm during modification of OC600, OC1000 and OC1500, respectively. The results of FTIR, TG and SEM analyses also implied that the clay mineral lost its hydrophilic character and gained organophilic features in OC600, OC1000 and OC1500. Additionally, these organoclays exhibited increased thermal stability, which makes them compatible with polymers.

Furthermore, the use of NC, OC600, OC1000 and OC1500 was examined in polyurethane foam fabrication considering its wide range of application fields in the polymer industry and promising aspects for new nanocomposite development. In these polymers, 2% by mass organoclay or NC was added into the structure of the PU foam by means of in situ polymerization, and one PUNC and three different PUOC nanocomposite samples were developed. The thermal stabilities of the in situ produced PUOC samples were noticeably improved compared to the PU control. Random and even distribution of the organically modified clay mineral in the host polymers was detected by SEM-EDS analysis. By comparison of DMA compression tests of the PU control and PUOC600, we demonstrated that the elastic behavior of PUOC600 could be improved, which was indicated by both the higher elastic modulus and lower $\tan \delta$ values when the force was applied in the range of 1–10 N at ambient temperature.

Consequently, the organoclay production presented in this study is presented as an easy and effective modification route for the intercalation of Na-MMT minerals using non-toxic, inexpensive and environmentally friendly PEGs of low molecular weight. The produced organoclay samples are quite suitable for the development of PU rigid nanocomposites with high thermal and mechanical performance.

Acknowledgments

This work was based on research project 107M126, which was funded by the Scientific & Technical Research Council of Turkey (TUBITAK). We also thank Istanbul Kultur University for financial support.

References

- [1] J.W. Gilman, Flammability and thermal stability studies of polymer layered-silicate (clay) nanocomposites, *Appl. Clay Sci.* 15 (1–2) (1999) 31–49.
- [2] A.B. Morgan, J.W.L.L. Chu, J.D. Harris, A flammability performance comparison between synthetic and natural clays in polystyrene nanocomposites, *Fire Mater.* 29 (4) (2005) 213–229.
- [3] G. Beyer, Nanocomposites offer new way forward for flame retardants, *Plast. Addit. Compd.* 7 (5) (2005) 32–35.
- [4] X. Zheng, C.A. Wilkie, Flame retardancy of polystyrene nanocomposites based on an oligomeric organically-modified clay containing phosphate, *Polym. Degrad. Stab.* 81 (3) (2003) 539–550.
- [5] F. Chavarria, D.R. Paul, Morphology and properties of thermoplastic polyurethane nanocomposites: effect of organoclay structure, *Polymer* 47 (22) (2006) 7760–7773.
- [6] Z. Wang, T.J. Pinnavaia, Nanolayer reinforcement of elastomeric polyurethane, *Chem. Mater.* 10 (12) (1998) 3769–3771.
- [7] H.K. Jeong, W. Krych, H. Ramanan, S. Nair, E. Marand, M. Tsapatsis, Fabrication of polymer/selective-flake nanocomposite membranes and their use in gas separation, *Chem. Mater.* 16 (20) (2004) 3838–3845.
- [8] B. Xu, Q. Zheng, Y. Song, Y. Shanguan, Calculating barrier properties of polymer/clay nanocomposites: effects of clay layers, *Polymer* 47 (8) (2006) 2904–2910.
- [9] Y. Zhong, D. Janes, Y. Zheng, M. Hetzer, D. De Kee, Mechanical and oxygen barrier properties of organoclay–polyethylene nanocomposite films, *Polym. Eng. Sci.* 47 (7) (2007) 1101–1107.
- [10] T. Ogasawara, Y. Ishida, T. Ishikawa, T. Aoki, T. Ogura, Helium gas permeability of montmorillonite/epoxy nanocomposites, *Composites Part A* 37 (12) (2006) 2236–2240.
- [11] P.J. Yoon, T.D. Fornes, D.R. Paul, Thermal expansion behavior of nylon 6 nanocomposites, *Polymer* 43 (25) (2002) 6727–6741.
- [12] A.K. Barick, D.K. Tripathy, Thermal and dynamic mechanical characterization of thermoplastic polyurethane/organoclay nanocomposites prepared by melt compounding, *Polym. Adv. Technol.* (2009), <http://dx.doi.org/10.1002/pat.1507>.
- [13] A.A. Vassiliou, K. Chrissafis, D.N. Bikiaris, In situ prepared PET nanocomposites: effect of organically modified montmorillonite and fumed silica nanoparticles on PET physical properties and thermal degradation kinetics, *Thermochim. Acta* 500 (2010) 21–29.
- [14] S.S. Ray, K. Okamoto, M. Okamoto, Structure–property relationship in biodegradable poly(butylene succinate)/layered silicate nanocomposites, *Macromolecules* 36 (7) (2003) 2355–2367.
- [15] S.S. Ray, K. Yamada, M. Okamoto, K. Ueda, Polylactide-layered silicate nanocomposite: a novel biodegradable material, *Nano Lett.* 2 (10) (2002) 1093–1096.
- [16] R.A. Vaia, S. Vasudevan, W. Krawiec, L.G. Scanlon, E.P. Giannelis, New polymer electrolyte nanocomposites: melt intercalation of poly(ethylene oxide) in mica-type silicates, *Adv. Mater.* 7 (1995) 154–156.
- [17] J.C. Hutchison, R. Bissessur, D.F. Shriver, Conductivity anisotropy of polyphosphazene–montmorillonite composite electrolytes, *Chem. Mater.* 8 (8) (1996) 1597–1599.
- [18] A. Usuki, Y. Kojima, M. Kawasumi, A. Okada, Y. Fukushima, T. Kurauchi, O. Kamigaito, Synthesis of nylon 6-clay hybrid, *J. Mater. Res.* 8 (5) (1993) 1179–1184.
- [19] Y. Kojima, A. Usuki, M. Kawasumi, A. Okada, Sorption of water in nylon 6-clay hybrid, *J. Appl. Polym. Sci.* 49 (7) (1993) 1259–1264.
- [20] Y. Kojima, K. Fukumori, A. Usuki, A. Okada, T. Kurauchi, Gas permeabilities in rubber–clay hybrid, *J. Mater. Sci. Lett.* 12 (12) (1993) 889–890.
- [21] J. Markarian, Automotive and packaging offer growth opportunities for nanocomposites, *Plast. Addit. Compd.* (2005) 18–25.
- [22] T. Glaskova, A. Aniskevich, Moisture absorption by epoxy/montmorillonite nanocomposite, *Compos. Sci. Technol.* 69 (2009) 2711–2715.
- [23] P. Camargo, H.C. Pedro, K.G. Satyanarayana, F. Wypych, Nanocomposites: synthesis, structure, properties and new application opportunities, *Mater. Res.* 12 (1) (2009) 1–39.
- [24] M.C. Roco, Broader societal implications of nanotechnology, *J. Nanopart. Res.* 5 (2003) 181–189.
- [25] F. Gao, Clay/polymercomposites: the story, *Mater. Today* 7 (11) (2004) 50–55.
- [26] B. Liao, M. Song, H. Liang, Y. Pang, Polymer layered silicate nanocomposites, *Polymer* 42 (2001) 10007–10011.
- [27] L.B. de Paiva, A.R. Morales, R. Francisco, D. Valenzuela, Organoclays: properties, preparation and applications, *Appl. Clay Sci.* 42 (2008) 8–24.
- [28] K.I. Breakwell, J. Homer, M.A.M. Lawrence, W.R. McWhinnie, Studies of organophilic clays: the distribution of quaternary ammonium compounds on clay surfaces and the role of impurities, *Polyhedron* 14 (1995) 2511–2518.
- [29] G.W. Beall, M. Goss, Self-assembly of organic molecules on montmorillonite, *Appl. Clay Sci.* 27 (2004) 179–186.
- [30] W.H. Awad, J.W. Gilman, M. Nyden, R.H.T. Harris, E. Sutto, J. Callahan, P.C. Tru-vole, H.C. DeLong, D.M. Fox, Thermal degradation studies of alkyl-imidazolium salts and their application in nanocomposites, *Thermochim. Acta* 409 (2004) 3–11.
- [31] F.A. Bottino, E. Fabbri, I.L. Fragalà, G. Malandrino, A. Orestano, F. Pilati, A. Pollicino, Polystyrene–clay nanocomposites prepared with polymerizable imidazolium surfactants, *Macromol. Rapid Commun.* 24 (18) (2003) 1079–1084.
- [32] H.A. Patel, R.S. Somani, H.C. Bajah, R.V. Jasra, Preparation and characterization of phosphonium montmorillonite with enhanced thermal stability, *Appl. Clay Sci.* 35 (2007) 194–200.

- [33] E. Naveau, C. Calberg, C. Detrembleur, S. Bourbigot, C. Jerome, Supercritical CO₂ as an efficient medium for layered silicate organomodification, *Polymer* 50 (2009) 1438–1446.
- [34] S. Mathur, B.M. Moudgil, Adsorption mechanism(s) of poly(ethylene oxide) on oxide surfaces, *J. Colloid Interf. Sci.* 196 (1997) 92–96.
- [35] S. Burchill, P.L. Hall, R. Harrison, M.H.B. Hayes, J.I. Langford, W.R. Livingston, R.J. Smedley, D.K. Ross, J.J. Tuck, Smectite–polymer interactions in aqueous systems, *Clay Miner.* 18 (4) (1983) 373–397.
- [36] C.C. Su, Y.H. Shen, Effects of poly(ethylene oxide) adsorption on the dispersion of smectites, *Colloids Surf. A: Physicochem. Eng. Aspects* 312 (2008) 1–6.
- [37] C.C. Su, Y.H. Shen, Adsorption of poly(ethylene oxide) on smectite, *J. Colloid Interf. Sci.* 332 (2009) 11–15.
- [38] R.L. Parfitt, D.J. Greenland, Adsorption of poly(ethylene glycols) on clay minerals, *Clay Miner.* 8 (1970) 305–306.
- [39] Z. Shen, G.P. Simon, Y.B. Cheng, Comparison of solution intercalation and melt intercalation of polymer–clay nanocomposites, *Polymer* 43 (2002) 4251–4260.
- [40] P. Aranda, E. Ruiz-Hitzky, Poly(ethylene oxide)–silicate intercalation materials, *Chem. Mater.* 4 (6) (1992) 1395–1403.
- [41] S. Rossi, P.F. Luckham, T.F. Tadros, Influence of non-ionic polymers on the rheological behaviour of Na⁺-montmorillonite clay suspensions—I Nonylphenol–polypropylene oxide–polyethylene oxide copolymers, *Colloids Surf. A: Physicochem. Eng. Aspects* 201 (2002) 85–100.
- [42] D.J. Chaiko, New poly(ethylene oxide)–clay composites, *Chem. Mater.* 15 (2003) 1105–1110.
- [43] Z. Shen, G.P. Simon, Y.B. Cheng, Saturation ratio of poly(ethylene oxide) to silicate in melt intercalated nanocomposites, *Eur. Polym. J.* 39 (2003) 1917–1924.
- [44] M.Y. Hikosaka, S.H. Pulcinelli, C.V. Santilli, K. Dahmouche, A.F. Craievich, Montmorillonite (MMT) effect on the structure of poly(oxyethylene) (PEO)–MMT nanocomposites and silica–PEO–MMT hybrid materials, *J. Non-Cryst. Solids* 352 (32–35) (2006) 3705–3710.
- [45] T.K. Kim, B.K. Kim, Y.S. Kim, Y.L. Cho, S.Y. Lee, Y.B. Cho, J.H. Kim, H.M. Jeong, Properties of reactive hot melt adhesives modified by polyurethane containing PEG segment intercalated in sodium montmorillonite, *Int. J. Mater. Form.* 1 (2008) 615–618.
- [46] P. Tzavalas, V.G. Gregoriou, Infrared spectroscopy as a tool to monitor the extent of intercalation and exfoliation in polymer clay nanocomposites, *Vib. Spectrosc.* 51 (2009) 39–43.
- [47] Y. Deng, J.B. Dixon, G.N. White, Bonding mechanisms and conformation of poly(ethylene oxide)-based surfactants in interlayer of smectite, *Colloid Polym. Sci.* 284 (2006) 347–356.
- [48] L. Zampori, P. Gallo Stampino, C. Cristiani, G. Dotelli, P. Cazzola, Synthesis of organoclays using non-ionic surfactants: effect of time, temperature and concentration, *Appl. Clay Sci.* 48 (2010) 97–102.
- [49] F. Zhao, C. Wana, X. Bao, B. Kandasubramanian, Modification of montmorillonite with aminopropylisooctyl polyhedral oligomeric silsesquioxane, *J. Colloid Interf. Sci.* 333 (2009) 164–170.
- [50] S.J. Tsipursky, D.D. Eisenhour, G.W. Beall, M. Clarey, J. Edwards, Method of determining the composition of clay deposit, US Pat. 6,235,533, 2001, Available from <http://patft.uspto.gov> and <http://www.nanocor.com>.
- [51] W. Xiea, Z. Gao, K. Liu, W.-P. Pa, R. Vaia, D. Hunter, A. Singh, Thermal characterization of organically modified montmorillonite, *Thermochim. Acta* 367–368 (2001) 339–350.
- [52] L. Caoa, J. Leea, T. Widyab, C. Macosko, Polyurethane/clay nanocomposites foams: processing, structure and properties, *Polymer* 46 (2005) 775–783.
- [53] G. Harikrishnan, T. Umasankar Patro, D.V. Khakhar, Polyurethane foam–clay nanocomposites: nanoclays as cell openers, *Ind. Eng. Chem. Res.* 45 (2006) 7126–7134.